Utah State University

From the SelectedWorks of Bela G. Fejer

May 1, 1986

The Condorequatorial spread-F campaign: Overview and results of the large-scale measurements

M. C. Kelley
J. LaBelle
E. Kudeki
Bela G. Fejer, *Utah State University*
S. Basu, et al.

Available at: https://works.bepress.com/bela_fejer/145/

bepress™

JOURNAL OF GEOPHYSICAL RESEARCH, VOL. 91, NO. A5, PAGES 5487–5503, MAY 1, 1986

The Condor Equatorial Spread *F* Campaign: Overview and Results of the Large-Scale Measurements

M. C. KELLEY,[1] J. LABELLE,[1] E. KUDEKI,[1,2] B. G. FEJER,[1] SA. BASU,[3,4] SU. BASU,[3] K. D. BAKER,[5] C. HANUISE,[6] P. ARGO,[7] R. F. WOODMAN,[8] W. E. SWARTZ,[1] D. T. FARLEY,[1] AND J. W. MERIWETHER, JR.[9]

During the Condor campaign a number of instruments were set up in Peru to support the rocket experiments. In this series of papers we report on the results of the experiments designed to study the equatorial *F* region. In this overview paper we summarize the main results as well as report upon the macroscopic developments of spread *F* as evidenced by data from backscatter radars, from scintillation observations, and from digital ionosonde meaurements. In this latter regard, we argue here that at least two factors other than the classical gravitational Rayleigh-Taylor plasma instability process must operate to yield the longest-scale horizontal organization of spread *F* structures. The horizontal scale typical of plume separation distances can be explained by invoking the effect of a shear in the plasma flow, although detailed comparison with theory seems to require shear frequencies a bit higher than observations indicate. On the other hand, the largest-scale organization or modulation of the scattering layer cannot be explained by the shear theory and must be due to local time variations in the ionospheric drift or to gravity wave induced vertical motions. Using simultaneous rocket and radar data, we were also able to confirm the oft quoted hypothesis that rapid overhead height variations in the scattering region over Jicamarca are primarily spatial structures advecting overhead. The detailed rocket-radar comparison verified several other earlier results and speculations, particularly those made in the PLUMEX experiments. In particular, companion papers discuss and extend some of the PLUMEX results to include the role of anomalous diffusion (LaBelle et al., this issue) in the theory of equatorial spread *F* and to shed light upon the shallow spectral form often observed in the intermediate-scale regime (LaBelle and Kelley, this issue).

1. INTRODUCTION

Equatorial *F* region irregularities, also known as equatorial spread *F* or ESF, have been studied extensively over the last few decades with a variety of experimental techniques including radars, scintillations, radio sounders, in situ rocket and satellite detectors, and a number of theoretical methods. Recent reviews of the topic include those by *Fejer and Kelley* [1980], *Ossakow* [1981], *Kelley and McClure* [1981], *Kelley* [1985], and *Basu and Basu* [1985].

As a part of project Condor a variety of instruments were clustered together near the magnetic equator to perform coordinated measurements of the same spread *F* events simultaneously. The idea behind the "cluster technique" is to learn more from a set of simultaneous measurements than can be learned from the individual experiments operated independently. The instruments used, along with their locations and operating institutions, are listed in Table 1. The locations are also indicated on the map in Figure 1. Two Terrier-Malemute rockets instrumented with electric field, plasma density, and energetic particle detectors were launched from the Punta Lobos Rocket Range (1 in Figure 1) in the approximately southward and southwestward trajectories indicated in Figure 1. The Jicamarca Radio Observatory (JRO), located to the north of the rocket range (2), provided continuous monitoring of 3-meter (3-m) *F* region irregularities with backscatter power and interferometric drift velocity measurements at an operation frequency of 50 MHz. At Ancon (3) a 14-MHz HF radar was operated to monitor the evolution of 10-m density irregularities. Scintillations and spaced receiver drift measurements were also conducted at the same location using several satellite transmissions. Analog and digital ionosonde measurements were conducted at the Huancayo station (4) (where VHF and UHF scintillation measurements were also performed), while Fabry-Perot measurements of neutral winds were made at Arequipa (just south of the region shown in Figure 1). The rocket project was a joint undertaking by the National Aeronautics and Space Administration of the United States and the Comission Nacional de Investigacion y Desarrollo Aerospacial (CONIDA) of Peru, and the JRO operations were a joint effort by the Instituto Geofisico del Peru and the National Science Foundation of the United States. A number of other results from Condor dealing with the equatorial electrojet, the critical velocity effect, middle atmospheric electrodynamic, etc., are published elsewhere.

The equatorial spread *F* aspects of the Condor project form part of a series of similar projects, which utilized simultaneous rocket and radar probing of the disturbed equatorial *F* region ionosphere. The series began on 1972 in India [*Balsley et al.*, 1972] and was followed by campaigns in Brazil [*Kelley et al.*, 1976], Peru [*Morse et al.*, 1977], Kwajalein [*Szuszczewicz et al.*, 1980], and India (S. Prakash, personal communication, 1983). During this same interval, great theoretical advances have occurred, particularly with respect to computer simula-

[1] School of Electrical Engineering, Cornell University, Ithaca, New York.
[2] Now at Department of Electrical Engineering, University of Illinois, Urbana.
[3] Emmanuel College, Boston, Massachusetts.
[4] Now at Air Force Geophysics Laboratory, Hanscom Air Force Base, Massachusetts.
[5] Center for Atmospheric and Space Sciences, Utah State University, Logan.
[6] Laboratoire de Sondages Electromagnétiques de l'Environnement Terrestre, University of Toulon, France.
[7] Los Alamos National Laboratory, Los Alamos, New Mexico.
[8] Instituto Geofisico del Peru, Lima.
[9] Space Physics Research Laboratory, University of Michigan, Ann Arbor.

Copyright 1986 by the American Geophysical Union.

Paper number 5A8723.
0148-0227/86/005A-8723$05.00

TABLE 1. Instrumentation Used During Project Condor, With the Locations and Operating Institutions

Instrumentation	Location	Institution(s)
Two Terrier-Malemute rocket-borne payloads	Punta Lobos Rocket Range	NASA, CONIDA, Cornell University, Utah State University, University of Illinois
50-MHz radar	Jicamarca	Instituto Geofisico del Peru, Cornell University National Science Foundation
14-MHz radar	Ancon	University of Toulon
VHF and UHF scintillation	Ancon	Air Force Geophysical Laboratory
VHF spaced receiver system		
Digital ionosonde	Huancayo	Los Alamos National Laboratory
Fabry-Perot interferometer	Arequipa	University of Michigan
Ionogram records and magnetometer	Huancayo	Instituto Geofisico del Peru

tion of ESF. The rocket experiments mentioned above solidified the importance of the generalized Rayleigh-Taylor instability as the basic theoretical construct about which to understand equatorial spread *F*. In addition, the results of the latter campaign, which has often been referred to as the PLUMEX experiments (Plume Experiments; actually PLUMEX I and PLUMEX II since there were two rockets launched), brought to light some important new aspects of the ESF problem which were not included in the computer simulations. For example, *Kelley et al.* [1982*a*] and *Kelley* [1982] interpreted the electric field and density fluctuation spectra in the transitional wavelength ($\leq$200 m) range as due to a drift wave mode. This important result was supported by a similar detector on the same rocket [*Singh and Szuszczewicz*, 1984] but not, prior to Condor, in an independent geophysical event. Similarly, the PLUMEX data indicated that a density fluctuation spectral form may exist in the intermediate wavelength range which is quite different from that predicted by simulations [*Rino et al.*, 1981; *Kelley et al.*, 1982*b*]. Part of the purpose of the Condor ESF experiments was to verify and understand these important results and their implication for ESF theory. As we shall see, this was accomplished, and new insights were obtained concerning the crucial role played by anomalous diffusion in determining the nonlinear saturation of ESF [*LaBelle et al.*, this issue] and concerning the possible origins of the surprising shallow spectral form [*LaBelle and Kelley*, this issue].

The detailed results of the Condor coordinated *F* region experiments are reported in the series of papers published in this issue. In this paper we present an overview of the experimental results and in addition report on some new aspects of the large-scale organization of plasma during ESF which are based primarily upon the radar backscatter maps made during the course of the rocket launch operation. We also summarize some of the main conclusions of the set of experiments.

2. Data Presentation

2.1. *Backscatter Maps and Scintillation Measurements on Nights Without Rocket Launches*

Real-time measurements at the Jicamarca Radio Observatory of backscattered power from 3-m *F* region irregularities played a crucial role in the rocket launch decisions of the Condor spread *F* campaign. In such measurements the received backscattered power is proportional to the square of the amplitude of the field-aligned density irregularities which have wave vectors in the direction of the radar line of sight. The Jicamarca radar beam is pointed almost vertically, about 3° north of the on-axis position, to achieve perpendicularity to the geomagnetic field at *F* region altitudes [see *Woodman*, 1970]. Power maps similar in essence to those published elsewhere in the literature [e.g., *Woodman and LaHoz*, 1976] were generated in real time to monitor the spread *F* activity level during the campaign. When rocket launch decisions were taken, the radar operation was switched to the more versatile radar interferometer mode capable of measuring the power spectra of the radar echoes as well as the east-west drift velocity of the scattering centers [*Kudeki et al.*, 1981]. In this section we present Jicamarca data obtained on nights with no rocket launches. The interferometer mode was not used on these nights, and the data presentation is limited to the power maps shown in Figures 2*a*–2*c*.

The upper panel in each figure is the radar map, while the lower panel is a plot of the scintillation index (*SI*) expressed in decibel excursions [*Whitney et al.*, 1969] at a frequency of 1.694 gigahertz (GHz). The latter data were obtained at Ancon using the GOES 5 satellite transmissions with an ionospheric intersection point at 300 km altitude only 30 km west of the Jicamarca beam. This distance is equivalent to only 3–5 min of time difference between the corresponding structures causing scintillation and radar backscatter when the eastward ionospheric drift is taken into account. The relationship between *SI* and the commonly used S_4 index as obtained by *Whitney* [1974] is given in the Figure 2*a* caption. At such high frequencies the scintillations conform to weak scatter theories,

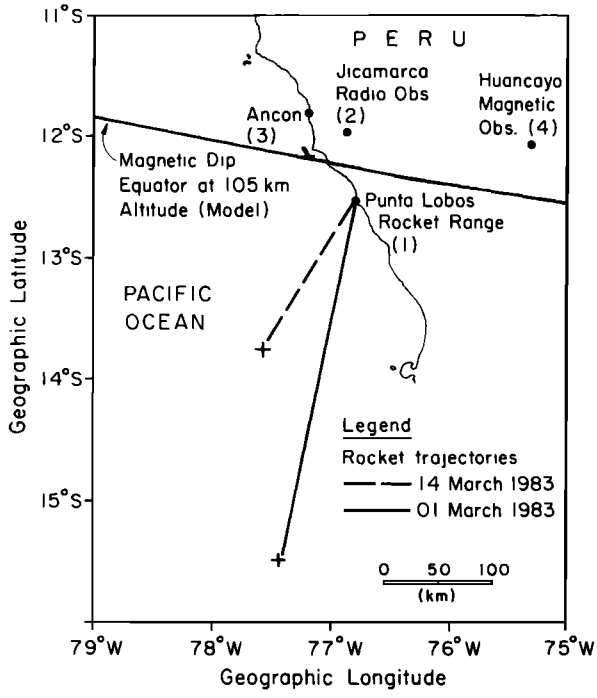

Fig. 1. Map of the coast of Peru, showing the trajectories of the two spread *F* rockets as well as the locations of various ground-based instrumentation.

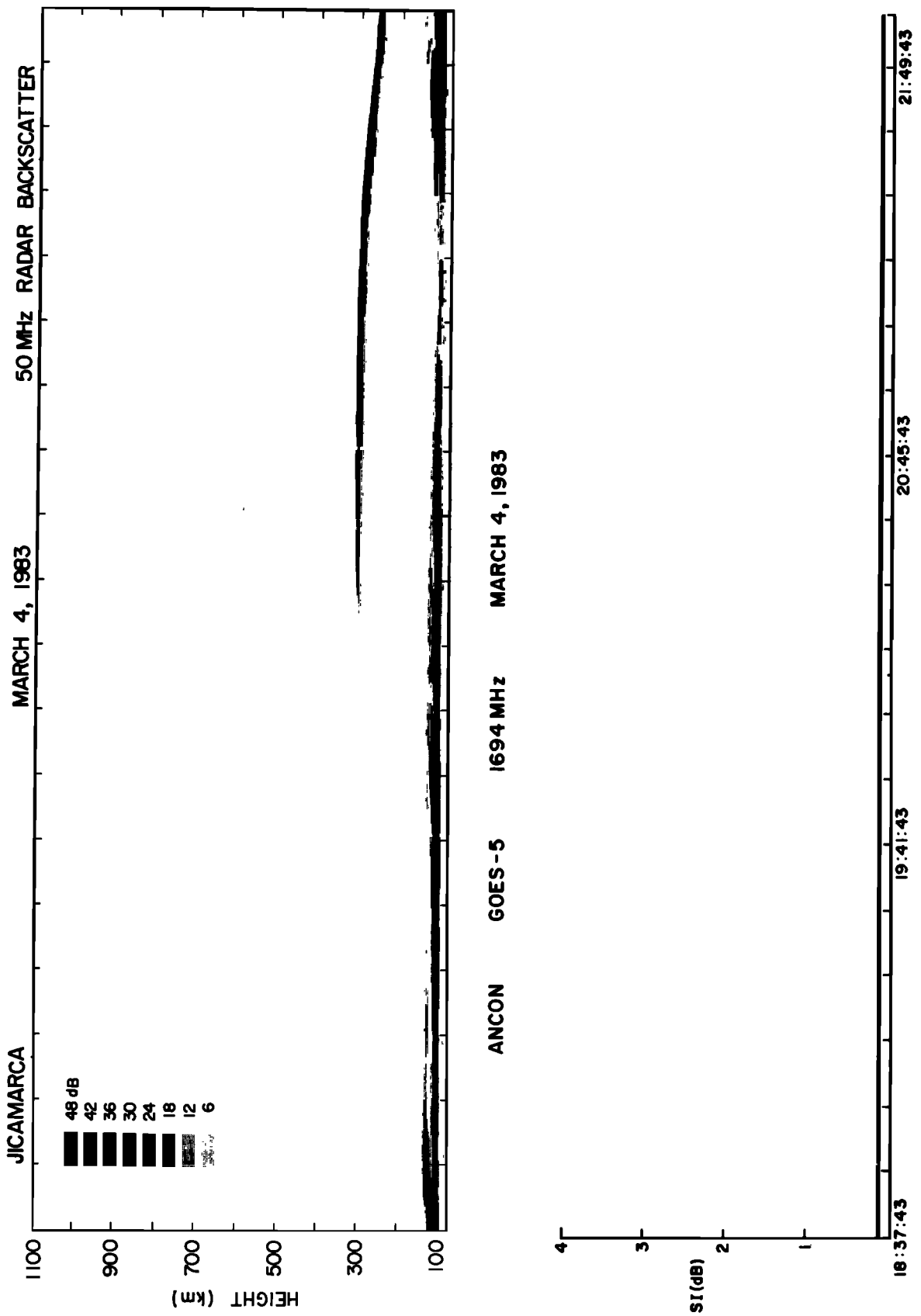

Fig. 2*a*. The top panel displays the backscatter power at 50 MHz observed at Jicamarca on the night of March 4, 1983, as a function of time and altitude. The bottom panel is a plot of the *SI* index of the 1694-MHz signal observed at Ancon. The *SI* index is the peak-to-peak signal fluctuation amplitude in decibels [*Whitney et al.*, 1969]. Some discrete relationships between *SI* and S_4 are 1 dB = 0.075, 3 dB = 0.17, 6 dB = 0.3, and 10 dB = 0.45.

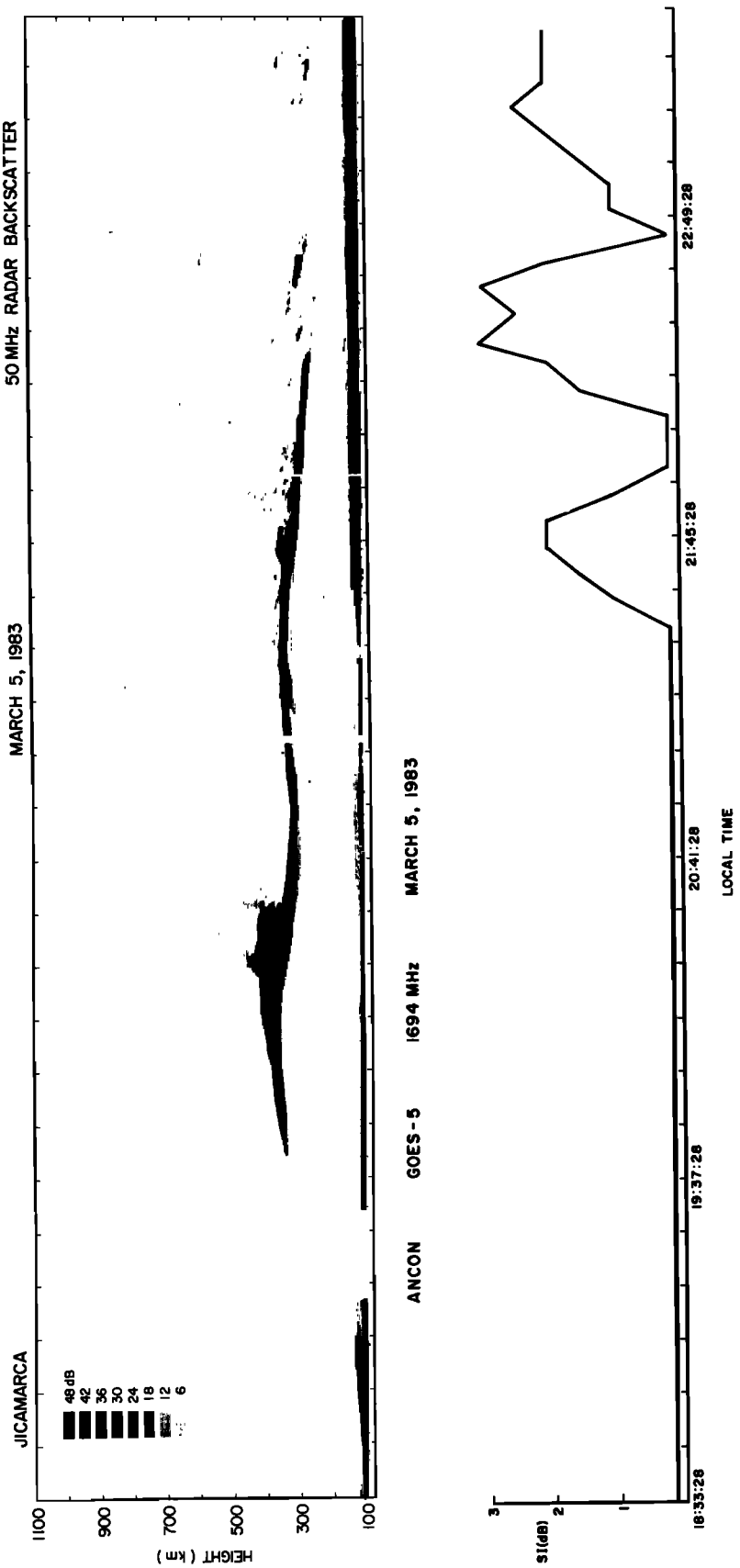

Fig. 2b. Same as Figure 2a, but for the night of March 5, 1983.

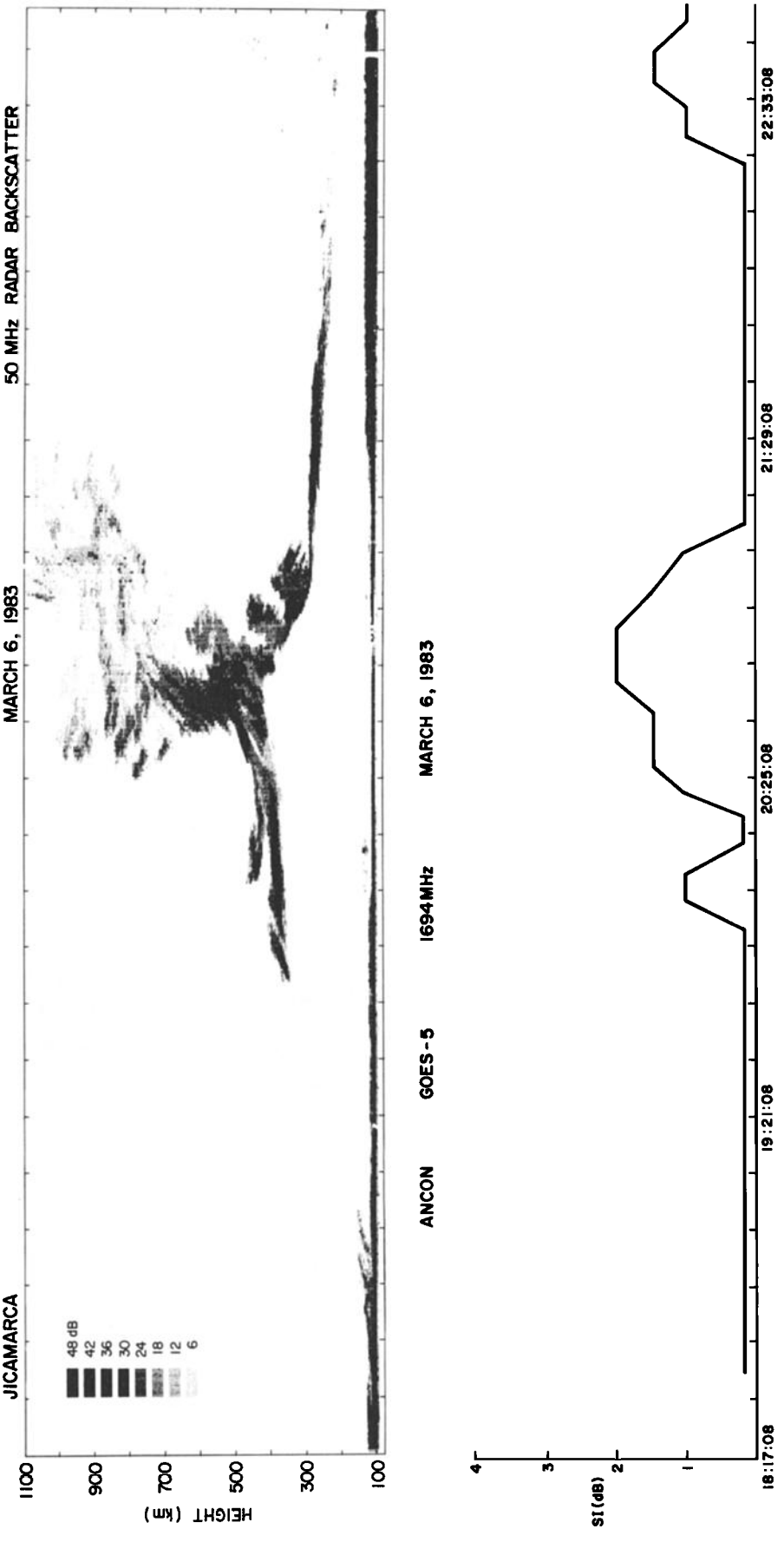

Fig. 2c. Same as Figure 2a, but for the night of March 6, 1983.

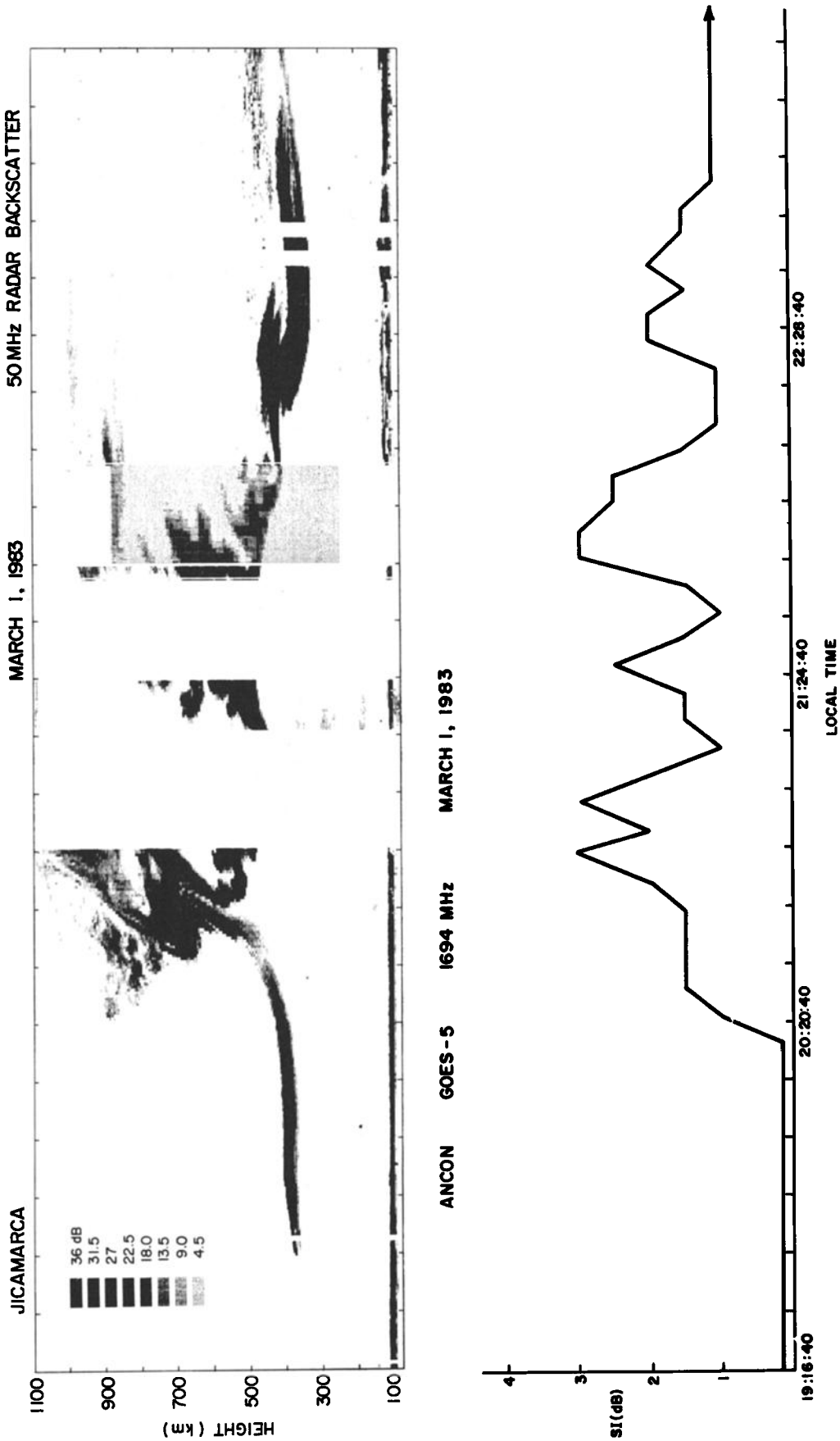

Fig. 3a. The top panel displays the Jicamarca 50-MHz backscatter power map recorder the night of March 1, 1983. The mottled portion around 2150 LT indicates the time period when the radar was operated in the interferometer mode, and the data gaps near 2104 LT and 2134 LT result from software tests which were conducted before the rocket launch. The bottom panel shows the scintillation index at 1694 MHz observed at Ancon during the same time period.

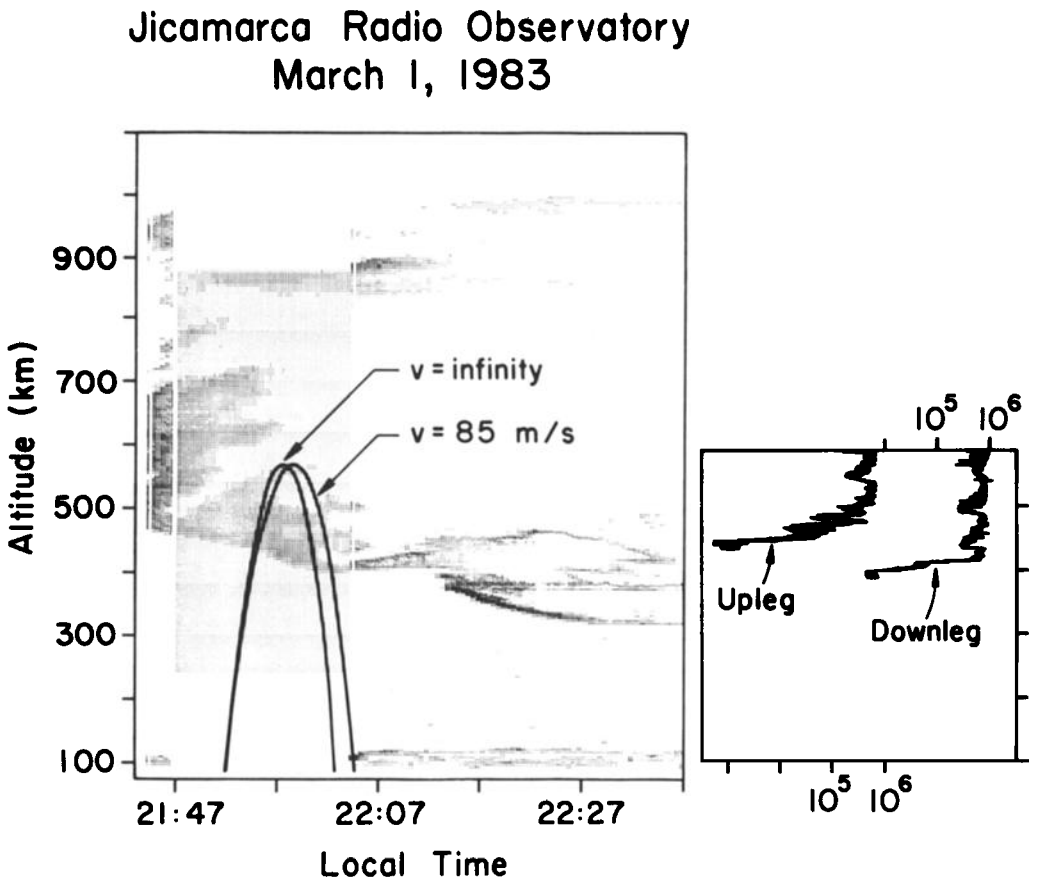

Fig. 3b. Expanded version of the Jicamarca radar power map with the rocket trajectory superposed. The inset at right illustrates the relative electron density profile obtained from a rocket-borne Langmuir probe. The densities listed assume a constant relationship between collected current and density equal to the value found near apogee on the second flight.

and a linear relationship holds between the S_4 index and the irregularity strength or electron density deviation (ΔN). At 1.7 GHz, scintillations are caused by irregularities in the range 35–350 m in dimension. We should therefore not expect a one-to-one relationship between 50-MHz backscatter, which is caused by 3-m irregularities, and the 1.7-GHz forward scatter.

In viewing the Jicamarca power maps it is important to remember that they provide vertical images or slices of the instantaneous overhead scattering structures which are then plotted as a function of time. A rigid scattering pattern drifting overhead with a constant velocity would be faithfully reproduced in these plots, and in this case the map can be considered as a view of the ionosphere looking southward. As pointed out by *Woodman and LaHoz* [1976], however, the technique is much like the slit cameras used in racing events which distort an image if it changes in time as it drifts by. In the description we try to remind the reader of this by using the words "apparent" to describe the motion of the scattering layer. Power maps display the echo power received by the Jicamarca radar, as functions of time and altitude, using a logarithmic gray scale coding. For each day a power level of 0 dB on these maps roughly corresponds to 3% of the estimated sky noise. There was no attempt made to maintain a uniform output power from day to day, but the scales differ by only ±6 dB.

The power maps of Figure 2 are representative of common types of spread *F* events observed at Jicamarca. In these plots the tick marks indicate 10.67 min (six ticks corresponding to 64 min). Throughout the discussion below, reference will be made to the local time at the 75° meridian—the time indicated in the plots. On March 4, 1983, a thin (10 km) scattering layer developed at about 2020 LT (Figure 2*a*). The position of the scattering layer was moving upward at an apparent velocity of about 2.5 m/s but never attained a height greater than 300 km. At "apogee" the layer broadened very slightly to a thickness of about 15 km. As the scattering layer descended, its thickness decreased. The structured echoing region near 100 km is due to 3-m irregularities excited by the equatorial electrojet instabilities. Notice that there are three gaps in the electrojet echoes at 2105, 2133, and 2141 LT when the *F* layer is hovering near its highest point. Furthermore, close inspection shows that the *E* layer scattering heights shift in altitude across the gaps as predicted by the linear electrojet theory when the zonal electric field changes sign [*Fejer et al.*, 1975]. This feature is fairly common, and the interpretation is that the *E* layer instabilities cease temporarily when the zonal electric field component passes through zero. Thus, even though the upward "motion" of the scattering layer is not a definitive measure of the actual vertical drift, the data are internally consistent with a pure bottomside *F* layer instability commencing while the *F* layer is rising and continuing virtually unchanged when the vertical drift reverses. The temporal behavior of the scattering height is also consistent with the well-established time dependence of the vertical drift velocity which creates a corresponding local time dependence of the ionospheric height. As the earth rotates under this local time de-

pendent feature, the ionosphere will seem to rise and then fall to a vertically looking radar. No detectable level of scintillation occurred at 1.7 GHz.

The March 5 night, illustrated in Figure 2*b*, was considerably more active than the previous example. The echoing layer started its development at an altitude higher than that on March 4. Just at and after "apogee" the layer broadened considerably, but no extended plumes developed, and the layer height decreased very quickly. The layer height then started to increase again, reaching 330 km before starting its final decrease for this evening. Notice that three distinct scattering patches developed in the second descending phase of the ionospheric oscillation and that the height oscillations were nearly sinusoidal in form. The characteristic gap in *E* region structure discussed above occurred only in conjunction with the second apogee, although the 100-km scattering layer became slightly more narrow in conjunction with the first apparent flow reversal. (When gaps occur in both the *E* and *F* region traces, they are due to a data loss.) The variations in altitude displayed on this night are much more rapid than those expected from the local time dependent zonal electric field effect described above. A number of weak 3-m scattering patches remained for a long time, including one between 500 and 600 km. The scintillation behavior on this night was very unusual; we return to this point after discussing the March 6 event.

On March 6 (Figure 2*c*) a spectacular plume event occurred over Jicamarca. The layered echoes commenced at 350 km altitude, considerably higher than on March 4. By 2010 LT the scattering layer was extended in altitude and displayed a bifurcated form. The height of the scattering layer increased abruptly at about 2025 LT, and shortly thereafter, a large plume event commenced which extended at times to more than 1000 km altitude. It is important to note that the highest-altitude scatterers were detected even before the plume feature was seen overhead between 400 and 600 km, and that three distinct miniplumes developed as the scattering layer descended. In this classic example of Murphy's law, a power failure occurred at the rocket range between 2025 and 2100 LT, precluding any rocket launch on this night.

At first glance, the scintillation data seem well correlated with the radar observations. A burst of strong gigahertz scintillation accompanied the bifurcation at 2010. This was followed by a long-lived event commencing at 2017 and lasting throughout the major plume event. The VHF scintillation index remained saturated during this event. At 2222 the scintillation level again rose dramatically, however, this time accompanied only by very weak patches of 3-m backscatter. One of these patches was centered at 360 km, even though the bottomside of the *F* layer was barely higher than 200 km at that time. The scintillation is nearly as strong as that associated with the plume itself and is more typical of previously published postmidnight events [*Basu et al.*, 1978]. Clearly the ~300-m structures are still very large in amplitude even though the 3-m waves have virtually disappeared.

Returning to the scintillation data on March 5, we note that the scintillation index reached values well above those associated with the major plume event on March 6 but were associated with only faint traces of 3-m backscatter. These patchy traces of 3-m backscatter were extended in altitude. Thus the pattern of scintillation data observed on March 5 resembles that observed late in the evening on March 6. It is possible that the first backscatter structure of the March 5 evening, characterized by an absence of scintillations, may have evolved directly over Jicamarca and drifted eastward so that it was not intercepted by the propagation path to the satellite. Similar events were discussed by *Aarons et al.* [1980].

2.2. *Data Obtained on March 1–2, 1983*

The backscatter power and scintillation data obtained on the evening of March 1–2, 1983, are presented in Figure 3*a*. This was the first night during which all the necessary radar analysis and display programs were functional, and some last minute testing led to the data gaps in the plot. The rectangular mottled area centered at about 2155 corresponds to the period when the radar was operated in the interferometer mode. In this mode the whole antenna array is used for transmission, but the backscattered signal is received independently by both the east and west quarters of the array, whose phase centers are separated by about 203 m. The phase difference between the simultaneous samples from these two quarters is related to the angular position of any localized scattering centers inside the common scattering volume. The east-west drift velocity of these localized scatterers is derived from the temporal changes of the measured positions [see *Kudeki et al.*, 1981; *Fejer et al.*, 1985]. Since vast amounts of raw data must be recorded for off-line processing, a smaller altitude range was sampled in the interferometer mode than in the power map modes before and after.

The figure shows an initial plume event centered at 2040 which followed a rapid apparent rise of the scattering layer and was preceded by high-altitude scatterers by some 10 min. Although the data gap creates some ambiguity, it appears that the layer descended and then began to rise once again at about 2120 LT, creating the second plume event into which the rocket was fired. The lower trace shows the results of simultaneous *L* band (1694 MHz) scintillation measurements performed at Ancon. Using the eastward *F* region drift speed measured by two independent methods (described below) for this night, the separation distance between these two measurements corresponds to only 3–5 min of local time difference. The data gaps are somewhat of a problem, but there again seems to be a good correlation between the *SI* index and the 3-m backscatter power. In particular, the thickness of the 3-m scattering patch and the magnitude of *SI* seem to be very well correlated. The backscatter map displays several "miniplumes" which extend like fingers pointing toward later local times (or pointing westward, if the features of these maps are considered frozen in the eastward drifting plasma). These features are similar to the secondary plumes detected with the Altair radar.

Figure 3*b* is an expanded version of the power map in Figure 3*a* and includes the rocket trajectory, which is plotted in two ways. The "V = infinity" parabola is plotted as though the radar and rocket observations were simultaneous in local time as well as in universal time. However, since the rocket traveled magnetically west of the radar while the ionosphere was drifting eastward, the rocket data at a certain time should be compared with the radar data a short time later, the exact time delay depending on the time it takes the ionospheric plasma to drift from the rocket's location to the longitude of Jicamarca [*Morse et al.*, 1977]. The second parabola includes the *F* region ionospheric drift of about 85 m/s as measured by the interferometer techniques during the shaded time period. Since the rocket trajectory also had a significant component magnetically southward, such a comparison relies upon the field-aligned nature of large-scale *F* region structures. *Tsunoda* [1981] has used the steerable incoherent scatter Altair radar to show that large-scale ($\simeq$50 km) features indeed do map along the magnetic field lines for large distances. Airglow data

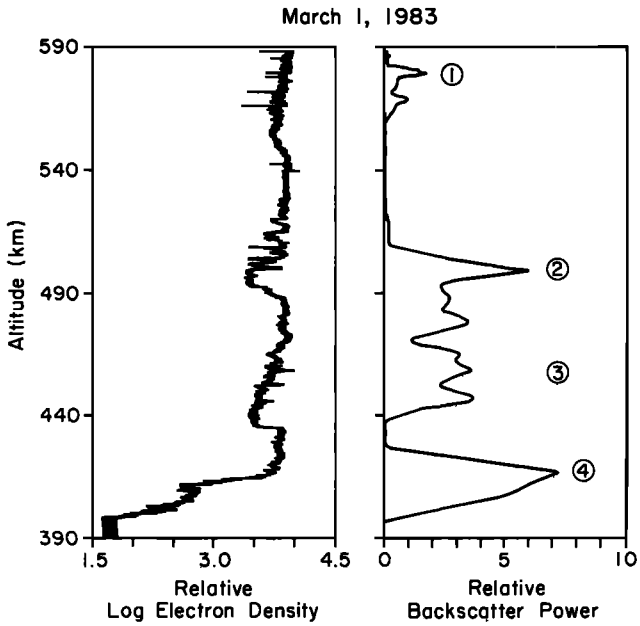

Fig. 4. Comparison between the relative electron density profile obtained from the rocket-borne probe and the relative backscatter power measured with the Jicamarca radar, which is sensitive to 3-m irregularities.

at conjugate off-equatorial latitudes also show this mapping quite clearly [*Mendillo and Tyler*, 1983].

The right-hand panel of Figure 3*b* displays electron current profiles detected by a fixed-bias Langmuir probe which are approximately proportional to the electron density. During the upleg of the rocket flight the steep upward gradient in plasma density and the associated irregularities observed at the bottomside of the *F* region coincide extremely well with the band of 3-m turbulence observed by the radar and first encountered by the rocket at 445 km altitude. On the downleg the lower edge as observed by the rocket-borne probe was nealy 40 km lower in altitude than on the upleg. This is in good agreement with the radar observations, which show that the layer height was decreasing over Jicamarca during this time. The small discrepancy between the downleg rocket data and the radar data can be explained quantitatively by the change in altitude of the field line which maps from the rocket's position to the latitude of Jicamarca. These data show conclusively that the bottom side of the *F* layer was higher over Jicamarca than at the rocket when it passed through the bottomside on the downleg. This implies that (1) a strong westward gradient in plasma density must exist and (2) for rapid height variations such as these the interpretation of the Jicamarca map in terms of a quasi-rigid motion of the scattering regions is valid at least for the bottomside.

In the topside the in situ probe detected several large regions of depleted electron density, along with associated smaller-scale irregularities. The amplitude of the depletions is about 50%, and their vertical size is in the range of 20–50 km. On the downleg, depletions of nearly identical properties were detected. On both downleg and upleg these depletions correspond one-to-one with the westward tilted miniplumes seen on the radar power map. Figure 4 illustrates more clearly this correlation between the depletions encountered by the rocket and the miniplumes in the radar backscatter power map. Only the downleg Langmuir probe data are plotted, and the altitude of the radar backscatter power has been adjusted in order to make a comparison more accurate, since the rocket moves magnetically south, intersecting field lines which map to higher altitudes at the equator above Jicamarca, as noted above. In Figure 4 an excellent correlation is observed between the radar backscatter power and those regions of upward directed density gradients detected by the rocket, as well as with the intermediate-scale fluctuations apparent to the eye in the rocket data.

Zonal plasma drift data are plotted in Figure 5 for both this day and the March 14–15 event discussed below. These velocity profiles were obtained using the Jicamarca radar interferometer procedure described by *Kudeki et al.* [1981]. Interferometer observations were made for about 15 min on each night, corresponding to the shaded regions in Figures 3*a* and

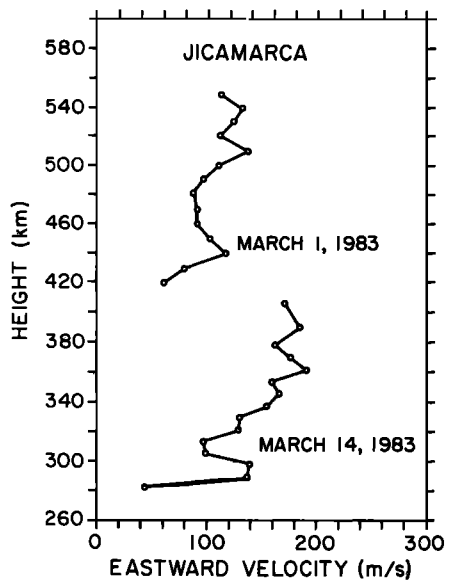

Fig. 5. *F* region zonal plasma drifts measured with the radar interferometer technique. Each curve represents the average profile during the periods indicated in Figures 3*a* and 8*a*.

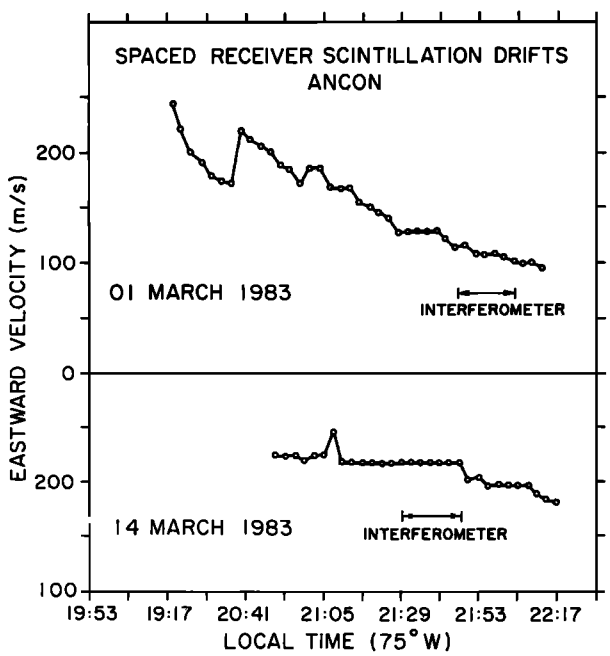

Fig. 6. Spaced receiver scintillation drifts measured at Ancon. The time periods of radar interferometer observations at Jicamarca plotted in Figure 5 are indicated.

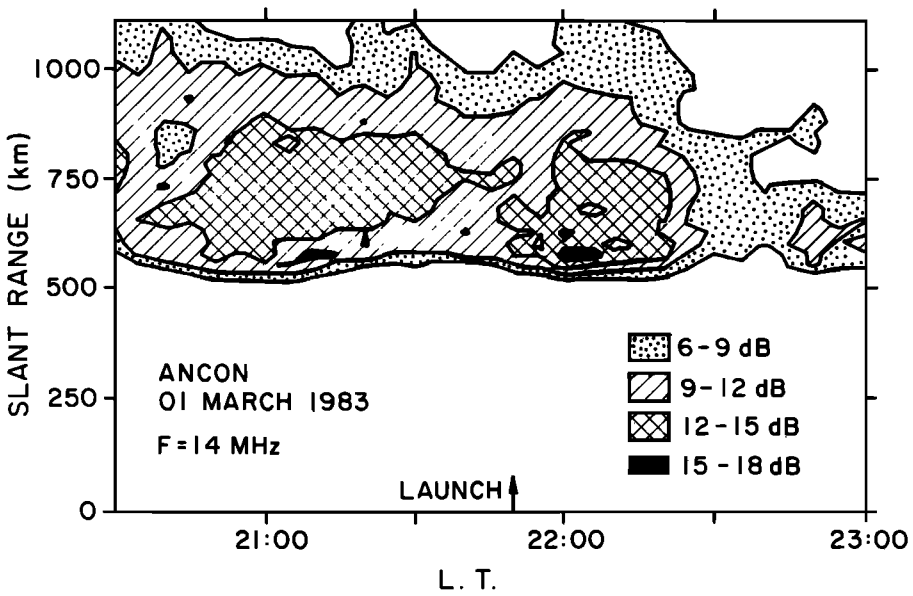

Fig. 7. Radar backscatter power measured with the 14-MHz radar at Ancon.

8*a*, but velocity measurements are only possible during periods and at heights where discrete scatterers are present. As a result, velocity estimates could not be made over the entire scattering region; velocities are plotted in Figure 5 only at altitudes for which discrete scatterers were present during at least 2 min of the 15-min interval, and in each case, the average value of drift velocity over the 15-min interval is plotted. The observed velocities are variable in time and height. On the night of March 1, 1983, the velocity in the region of the strongest echoes was about 90 m/s. A vertical shear in the zonal flow with mean value of 6×10^{-4} s^{-1} is indicated since the flow increases from about 60 m/s at 420 km to over 120 m/s at 520 km.

Drift measurements were also made using the spaced receiver scintillation technique which is sensitive to subkilometer irregularities. These measurements were made at 244 MHz with a short (123 m) and a long (246 m) baseline [*Basu and Whitney*, 1983]. The temporal variations of the apparent velocities during March 1 and March 14 are shown in Figure 6. The spaced receiver scintillation drifts are in fairly good agreement with the interferometer drifts on March 1 but are somewhat larger than the corresponding Jicamarca measurements made on March 14.

We turn now to HF backscatter measurements made at Ancon. A range-time-intensity plot of the echoes received at 14 MHz, corresponding to a backscatter wavelength of 10 m, is presented in Figure 7. In this experiment the antenna was directed upward, but because of the wide beam, echoes were obtained from angles $\pm 30°$ from vertical. It seems that the strongest HF scatter originates from the bottomside spread *F* at a slant range of about 550 km. This scatter corresponds to the strong echoes received at Jicamarca at around the same altitude. However, note that the shortest range at which 14-MHz echoes were received is somewhat longer than the lowest-altitude 3-m echoes observed by Jicamarca; this is probably an indication of the relative sensitivity of the two radars. The extension of the 14-MHz echoes to over 1000 km in range is due to oblique returns. Representative spectra at a fixed range (500 km) (not shown) are very narrow and display sequences of Doppler shifts which changed from negative to positive over the 1-hour period 2145–2245 LT. Because of the antenna beam width, this variation is most probably due to the horizontal motion of scatterers across the beam (the radar measures the radial line-of-sight velocity). If the scatterers which produce these spectra originate approximately from the same altitude as the strongest backscatter observed by Jicamarca, then the variation of the Doppler spectra as a function of time indicates an average drift velocity of about 100 m/s. This value agrees well with the interferometer and spaced receiver drift measurements. No digital ionosonde data were available on this night.

2.3. *Data Obtained on March 14–15, 1983*

Composite data presentations for the night of March 14–15 are given in Figures 8*a* and 8*b*. In this case, the electron density profile displayed in the inset of Figure 8*b* was obtained from two different rocket-borne instruments. An RF probe determined the absolute electron density by locking onto the local upper hybrid frequency in the plasma when the plasma density exceeded about 10^5 cm^{-3} [*Baker et al.*, 1969, 1985]. At lower densities the data profile was extended using the relative density measurement from the fixed-bias Langmuir probe, normalized to match the value of absolute density measured by the RF probe at 350 km.

The morphology of the March 14 event in many ways resembles the March 1 data set. The major difference is the altitude of the event. For example, the bottomside and *F* peak heights were more than 100 km lower on March 14–15. Once again, the steep upward gradient in plasma density and the associated irregularities observed at the bottomside of the *F* region coincide with the band of 3-m turbulence observed by the radar and encountered by the rocket between 290 and 340 km. A density depletion just below the *F* peak corresponds to the patch of 3-m irregularities at 360 km altitude. The scintillation index *SI* correlates well with the thickness of the backscatter region, although it commenced earlier than did the VHF scatter.

In the topside the in situ probe detected a distinct region of depleted electron density above 410 km altitude on the upleg. A nearly identical feature was observed on the downleg at a higher altitude. However, turning to the backscatter power

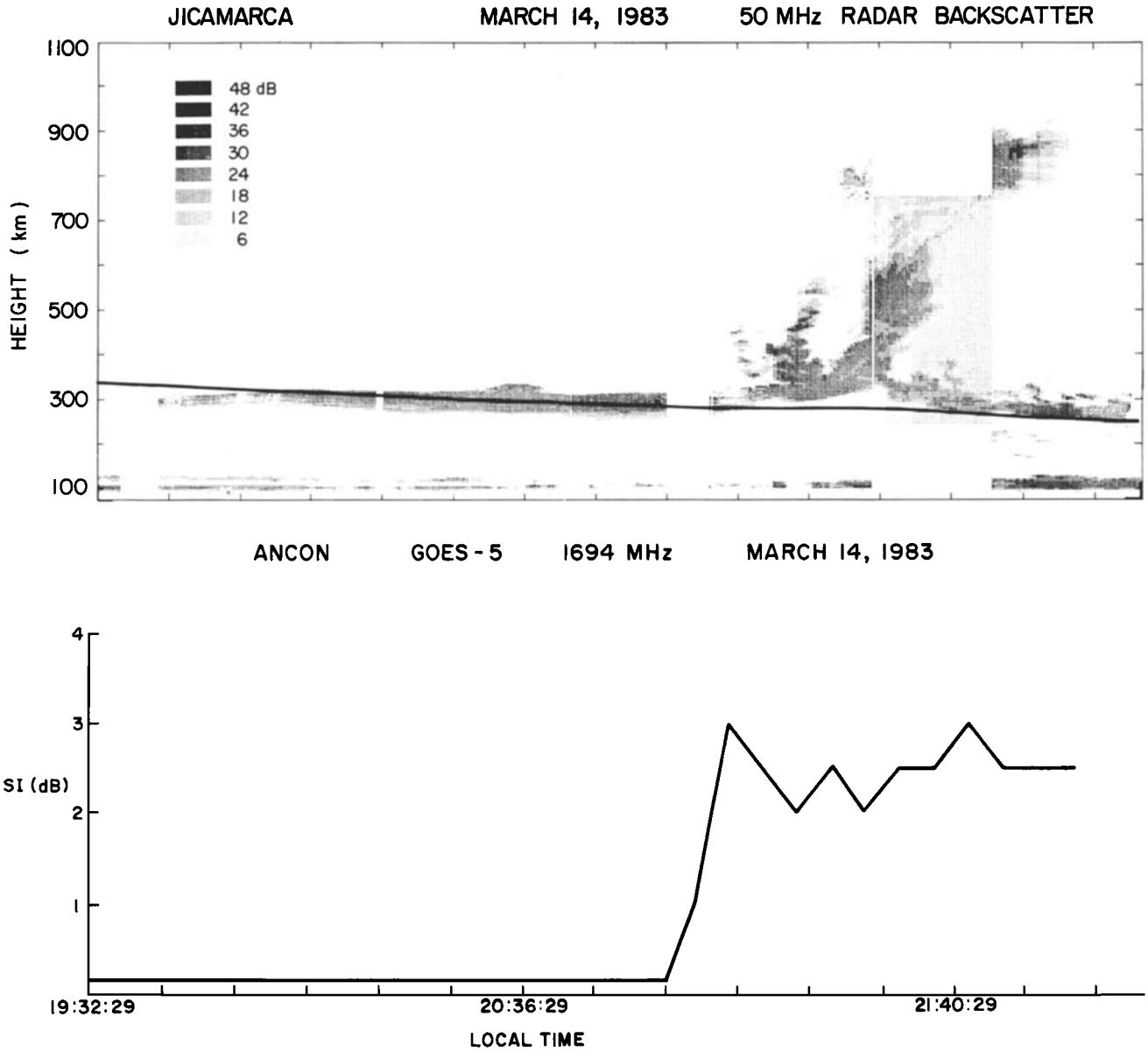

Fig. 8*a*. The top panel displays the Jicamarca 50-MHz backscatter power map recorded the night of March 14, 1983. The solid line indicates the altitude h_{min} as measured from the ionosonde at Huancayo. The bottom panel shows the scintillation index at 1694 MHz observed at Ancon during the same time period.

map, within the range of sensitivity of the Jicamarca radar, no 3-m irregularities are seen during the portions of the rocket trajectory described above; that is, the "bubble" observed by the rocket during both upleg and downleg apparently was invisible to the radar by the time it was overhead. However, at an earlier local time (2133 LT), Jicamarca did detect a westward tilted miniplume which, if extended, would intercept the rocket trajectory at about the right places. Furthermore, if we identify the upleg depletion with its downleg twin, observed 5 min later in local time and 40 km higher in altitude, there is a remarkable similarity to the March 1 data.

Interferometer drift data for this night were presented earlier in Figure 5 (upper trace). The observed drift again exhibits a strong vertical shear (8×10^{-4} s^{-1}), increasing from near 100 m/s to about 180 m/s over a 100-km height range. The comparison in Figure 6 shows that on both nights (March 1 and March 14), spaced-receiver drifts are higher than those measured by the interferometer. This seems to be a general feature of the spaced receiver technique. In addition, the interferometer drift measurements indicate that the zonal plasma drift velocity can change significantly with height and time. The spaced-receiver drifts, on the other hand, yield information on the region with the largest electron density fluctuations. This intercomparison is discussed in more detail in a companion paper [*Basu et al.*, this issue].

Figure 9 shows two spectra of the intermediate-scale density irregularities measured by the Utah State absolute density probe. The upper panel corresponds to turbulence in the topside well above the F peak, while the lower panel corresponds to the intense turbulence just above the peak in F region density. Comparison of the two spectra reveals a remarkable feature in the lower-altitude March 14 spectrum: the intermediate range of wavelengths is characterized by two distinct subranges, with a break in the spectrum near 1 km. The portion of the spectrum consisting of wavelengths smaller than about 1 km displays a k^{-n} form with spectral index $n \geq 2.5$,

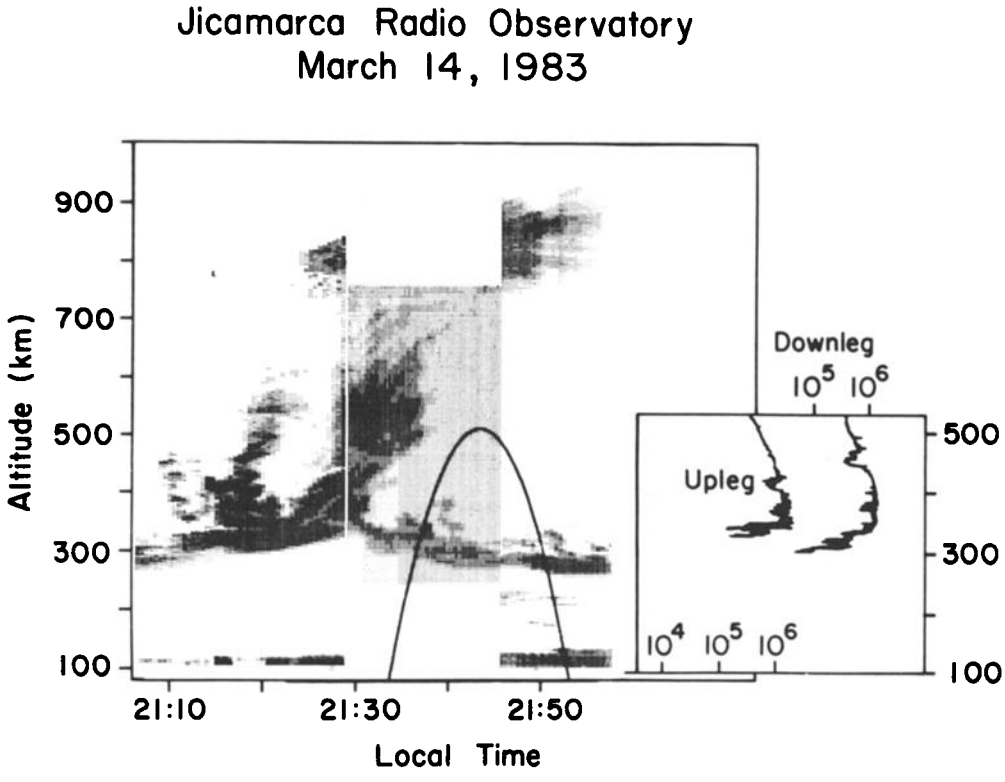

Fig. 8*b*. Expanded version of the Jicamarca radar power map with the rocket trajectory superposed. The inset at right shows the electron density profile obtained from the plasma frequency probe and extended using the Langmuir probe.

while for wavelengths longer than about 1 km the spectrum exhibits a smaller spectral index. This feature has been observed previously in in situ rocket spectra [*Rino et al.*, 1981], and there is some evidence for such a variation in the spectral index of satellite-measured spectra [*Livingston et al.*, 1981; *Basu et al.*, 1983]. The generation of enhanced turbulence near and above the kilometer scale in spread *F* and in scintillation spectra is examined in detail in a companion paper [*LaBelle and Kelley*, this issue]. This height region corresponds to one which had very broad VHF spectral signatures (wide Doppler spectra), which also suggests a very turbulent medium.

Data from the digital ionosonde located at Huancayo are included in Figure 8*a*, in which the altitude of the bottom of the *F* layer (h_{min}) over Huancayo has been superposed upon the Jicamarca backscatter map. Early in the evening the *F* layer is higher at Huancayo, with the roles reversing around 2030 LT. This is also the time when the 3-m scattering layer over JRO stalls in its slow upward drift. Notice that the brief increase in the irregularity layer thickness and the gap in *E* region irregularities occur at the same time as the reversal. The apparent drift observed by Jicamarca is consistent with a typical vertical drift morphology [*Fejer et al.*, 1979], in which the plasma moves upward at all local times before 2030 (on this night) and downward after this time. The ionospheric tilt associated with this morphology would have the Huancayo layer above the Jicamarca layer before 2030 and vice versa afterward, as observed. However, the apparent tilt is much more pronounced than the small longitude difference would imply, as discussed in detail in a companion paper [*Argo and Kelley*, this issue]. The abrupt uplift after 2100 is nearly simultaneous at both sites, suggesting that the associated eastward electric field extended over both Huancayo and Jicamarca.

3. Discussion of the Large-Scale Results

3.1. *Implications for the Large-Scale Development of Equatorial Spread F*

Interpretation of the Jicamarca radar backscatter map often uses the assumption that the relatively thin echoing regions correspond to the structured bottomside of the layer [e.g., *Kelley et al.*, 1981]. This important hypothesis is upheld in great detail by the combined rocket and radar data obtained during the upleg of both Condor rocket flights, as well as during the equatorial ionosphere (Equion) experiment [*Morse et al.*, 1977]. For example, the echoing layer is more than 100 km higher on March 14, as are the bottomside gradient and the *F* peak deduced from the rocket data.

Using this relatively firm assumption, we note immediately that widespread equatorial spread *F* develops only when the layer is high. For example, in Figure 2*a* the height of the echoing layer never exceeds 300 km and never exceeds 10 km in vertical extent. The layer seems to be rising when echoes first appear, and the backscatter signal continues virtually unchanged as the layer reverses, dying out as the echo height slowly comes down again. Conversely, the initial position of the structured *F* layer is highest on March 1, the night with the most sustained 3-m backscatter activity. This requirement has been noted previously [e.g., *Farley et al.*, 1970]. Plume development is also well correlated with layer height. *Kelley et al.* [1981] noted a distinct tendency for plumes to form either at layer "apogee" or when it seems to be descending. This is also upheld in detail by the present data set. The major plumes on March 1, 6, and 14 are all of the apogee type. Even in the relatively quiet 3-m backscatter observed on the evening

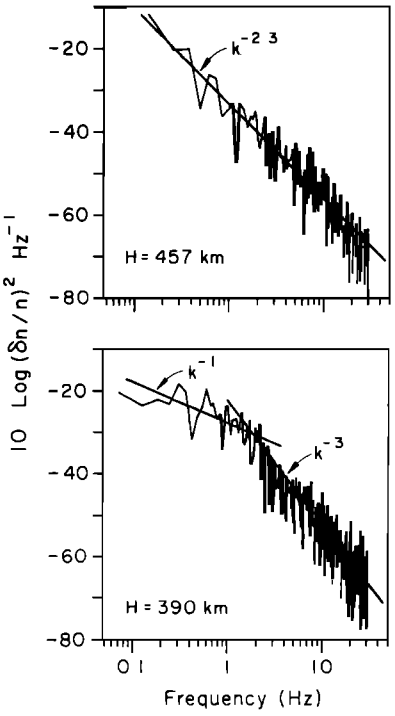

Fig. 9. Two examples of the spectrum of density fluctuations detected by the second Condor spread F rocket (March 14, 1983). The top panel corresponds to an altitude of 457 km, and the bottom panel corresponds to an altitude of 390 km.

of March 5, a plume seemed to almost develop at 2010 LT when the layer reached its peak altitude. A very similar "near-plume" feature was seen at 2030 LT on March 14. This result is very strong evidence for the importance of the gravitational term in the generalized Rayleigh-Taylor (GRT) instability [*Kelley et al.*, 1981] as the major controlling influence on equatorial spread F, since the growth rate is inversely proportional to the ion-neutral collision frequency (ν_{in}). Using a local value for ν_{in}, the growth rate due to a purely gravitationally driven process is given as a function of height approximately by the expression

$$\gamma_g \simeq 0.09 \exp [(h - 300)/50] \quad \text{min}^{-1}$$

in which we have assumed a vertical gradient scale length of 20 km and a neutral scale height of 50 km. This implies that the e-folding time for irregularity growth decreases from 11 to 4 min between 300 and 350 km. Of course, a feature as extensive as a plume cannot grow from thermal noise in a few e-folding times, so seed structure must be present at much larger scales than 3 m in the bottomside region as it drifts upward. Indeed, the rocket data reported by *Kelley et al.* [1976] and *Costa and Kelley* [1978] showed well-developed bottomside 1- to 4-km structures ($\delta n/n \approx 30\%$) in just such conditions, e.g., F peak at 300 km, slow 10-m/s uplift determined by barium cloud drifts, and weak 3-m structures which seemed to erupt into a plume a few minutes later.

The other terms in the GRT process, which involve electric fields and neutral winds as sources of free energy, do not depend upon the collision frequency and hence are not altitude dependent. These terms are not negligible, and the present data set confirms and extends several conclusions of *Kelley et al.* [1981] in this regard. First, we note the tendency for two types of ionospheric uplift. On March 5 (Figure 2*c*), three gentle wavelike undulations of the F layer are apparent. This is to be constrasted with the sharp uplifts at 2145 LT on March 1 (Figure 3*a*), at 2050 LT on March 6, and at 2128 LT on March 14. The first and third of these three examples followed a cycle of gentle wavelike undulations with the plume and associated rapid uplift seeming to feed upon the more gentle uplift. We first discuss the origin and effects of "gentle" undulations, returning to the other class in section 3.2.

Although data gaps confuse the issue somewhat, the March 1 data (Figure 3*a*) display as many as four wavelike oscillations, two of which are punctuated by apogee plumes. The apparent descending phase of such oscillations is often characterized by the development of several isolated plumes. It takes some imagination to see this on March 1, but on March 6 (Figure 2*b*), three such "postapogee" plumes occur. Even on the relatively quiet night of March 5 (Figure 2*c*) the second undulation has three separate regions in which the scattering layer broadens briefly, which are centered at 2145, 2154, and 2203 LT. In the spectacular event studied by *Kelley et al.* [1981], also, two plumes developed on the "descending phase" of both of two extreme oscillations ($\geq$300 km amplitude) recorded on March 21, 1979. Both of these major undulations had large apogee plumes.

The rocket data show definitely that ionospheric tilts can be significant and that the hypothesized tilt suggested by *Kelley et al.* [1981] is indeed the correct one when the scattering layer seems to rapidly descend over Jicamarca. The ionospheric orientation during such an event is such that the plasma density gradient has a westward component. The typical zonal wind direction for this local time sector is eastward [*Sipler and Biondi et al.*, 1978; *Meriwether et al.*, this issue]. Since the magnitude of the zonal wind component u must be larger than the eastward plasma drift velocity it generates by the F region dynamo effect, the vertical electric field in the neutral frame, $E_z' = E_z + uB$, must be upward. This further implies that $\mathbf{E}' \times \mathbf{B}$ has a component parallel to the westward zonal plasma density gradient mentioned above. This is a linearly unstable condition. The horizontal density gradient scale length can be estimated from the rocket data to be 14 km. For $E'/B \approx 100$ m/s this yields an exponential growth time of 2.3 min, which is very fast.

There are presently two competing theoretical explanations for the organization of equatorial spread F at the largest scales, gravity wave seeding, and velocity shear instabilities. By large scale we mean $\lambda \gg L$, the vertical density gradient scale length. *Kelley et al.* [1981] argued that the quasi-sinusoidal undulations were due to gravity wave seeding as described by *Klostermeyer* [1978]. Once seeded, such structures may then be amplified preferentially by a plasma instability process. In the other view, large-scale undulations are driven directly by a velocity shear instability. The advantage of the latter process over a Rayleigh-Taylor instability is that the growth rate peaks at $\lambda \geq L$ for the velocity shear instability whereas the opposite inequality holds for the Rayleigh-Taylor mode.

To investigate this further, we first study the spacing between multiple plumes such as those detected on March 6, 1983, while the scattering layer height is decreasing over Jicamarca. The usual assumption is that the spacing can be estimated by using a mean eastward plasma velocity $V_E = 150$ m/s and then converting the time Δt between events in terms of a distance L via $L = V_E \Delta t$. To test this methodology, we can use the scanning Altair radar on Kwajalein, for which

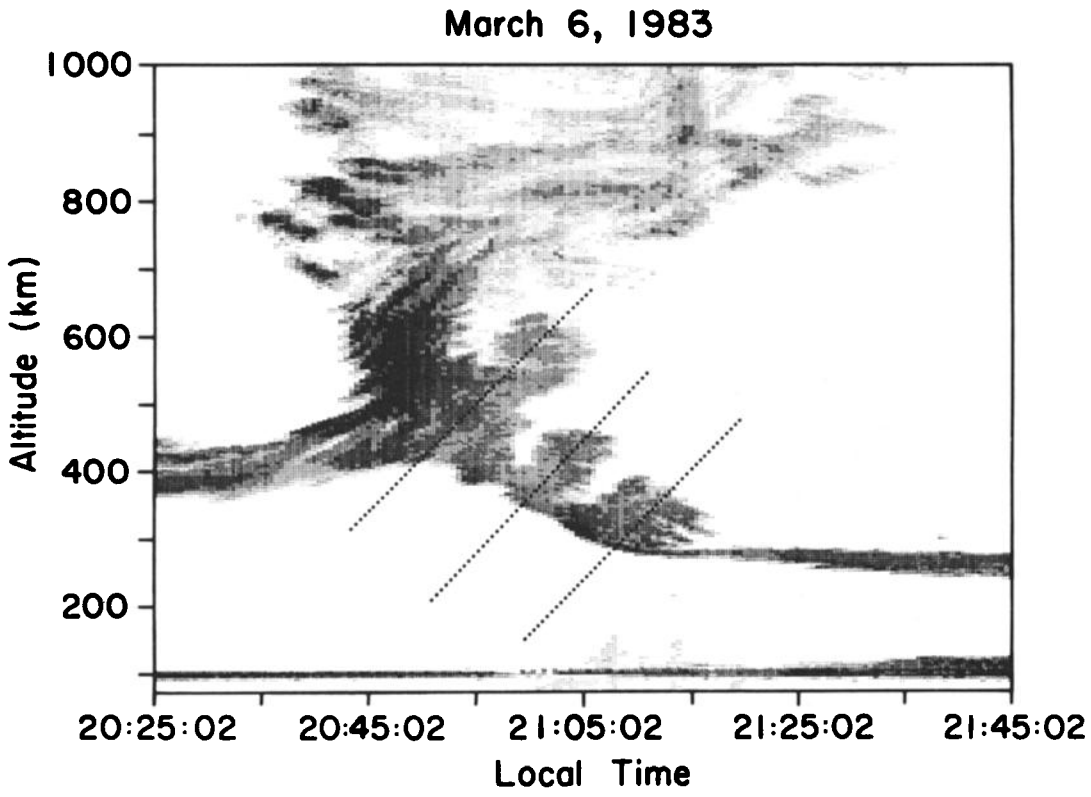

Fig. 10. The Jicamarca backscatter power map from the night of March 6, 1983, showing three prominent plume structures which erupt from the bottomside spread F as the scattering layer decends. Superposed are the relative positions of three similar structures observed using a scanning radar [*Tsunoda*, 1983].

there is not an ambiguous relationship between time and space, and compare the separation of multiple plumes measured there to the separations deduced from the Jicamarca data. To make this comparison, we have taken a scanning radar plot from Figure 2*b* of *Tsunoda* [1983], reversed it east-west, and plotted the position of his three multiple plumes over the March 6 event in Figure 10. As noted above, we assumed an eastward drift of 150 m/s to convert time to space in the Jacamarca plot. Notice that under this assumption the spacing of the Altair plumes is nearly identical to that registered by the Jicamarca radar.

We now use this method to investigate what seems to be a characteristic spacing between such plumes. From the March 1, 5, and 6 data we have determined four sets of spacings in time and converted them to spatial units (assuming a 150-m/s eastward velocity). Four more plume spacings were estimated from the data published by *Kelley et al.* [1981], and two more actual spacings determined from the work by *Tsunoda* [1983] discussed in the previous paragraph. The spacings d range from 91 to 206 km with a mean value of 150 km. In terms of the normalized wave number $\hat{k} = 2\pi L/d$, where L is the zero-order bottomside density gradient taken to be 20 km, these spacings correspond to the range $\hat{k} = 0.6$–1.38 with an average of $\hat{k} = 0.84$.

Guzdar et al. [1982] and *Satyanarayana et al.* [1984] have studied the generalized Rayleigh-Taylor process, including the effect on the growth rate of a vertical shear in the eastward plasma drift velocity. Although such a shear lowers the growth rate, it also moves the most unstable waves from a normalized $\hat{k} \simeq 10$ to values in the range 0.5–2, which is much more consistent with the spacings reported here. We thus might conclude that the shear is important in determining the outer horizontal scale of equatorial spread F. However, using the theory of *Satyanarayana et al.* [1984] and assuming that the wavelength of the maximum linear growth rate corresponds to the observed spacings, the range of $\hat{k}$ found above corresponds to plasma shears (dV_x/dx) in the range 2.6×10^{-2} to 6×10^{-3} s^{-1}. These shears are about 10 times the values indicated by Figure 5, as well as by other radar-based shear measurements [*Kudeki et al.*, 1981; *Tsunoda et al.*, 1981].

One possible way out of this dilemma is to conjecture that the shear is higher in a localized region within the plasma gradient than indicated by the radar data, say 100 m/s over a 10-km bottomside height range. Neutral wind shears of this magnitude have been reported [*Bhavsar et al.*, 1965]. Another possibility is that the dominant horizontal wave number in the fully developed process is smaller than the wave number of maximum growth. This might imply an inverse cascade of energy to larger scales in this two-dimensionally turbulent medium. A less exotic explanation is that although the growth rate is lower at small $\hat{k}$, the initial amplitude was higher and the longer-wavelength waves saturated earlier.

In summary, the present analysis supports the notion that velocity shear plays a role in determining the plume spacings which occur in the range $\hat{k} \approx 1$. However, it should be noted that to reach this conclusion, very high shears must be invoked. To push the shear explanation to even longer wavelengths, and hence to explain the "gentle undulations" of the F layer, does not seem at all realistic. We thus fall back upon the conclusions of *Kelley et al.* [1981] as well as *Röttger* [1973], *Klostermeyer* [1978], and many others, that gravity waves and their associated electric fields must organize the plasma at

scales of ≥ 200 km. This area is also discussed in some detail in the companion paper by *Argo and Kelley* [this issue].

3.2. *Wedges or Bubbles?*

It was originally conjectured that the plasma depletions associated with equatorial spread F may either pinch off, forming bubbles of low-density plasma, or be wedges linked to the bottomside by a region of low density [*Woodman and LaHoz*, 1976]. The radar structure linking the plume head to the bottomside, in the pinch model, was then due to a turbulent wake [*Woodman and LaHoz*, 1976; *Kelley and Ott*, 1978]. Recent experimental evidence [*Mendillo and Tyler*, 1983; *Tsunoda et al.*, 1982], theoretical calculations based on satellite data [*Hanson and Bamgboye*, 1984], and computer simulations by *Zalesak et al.* [1982] support the wedge concept.

Returning to Figure 3*b* comparison of the highest-altitude depletions on the two rocket profile shows that the downleg depletion was encountered well above the corresponding upleg event. This seems to imply that the depletion was located at a higher altitude west of Jicamarca. The radar data confirm this hypothesis. In Figure 3*b* an arrow points out a "miniplume" of 3-m echoes which intersects the parabola labeled $V = 85$ m/s at the same height as the uppermost depletion in the rocket plasma density profile. Although this echoing region was decaying in power with time over Jicamarca, the patch can also be seen to intersect the rocket parabola during its downleg at the height of the uppermost depletion in the rocket profile.

It would be remarkable indeed if a rocket penetrated two pinched-off bubbles along its trajectory, even allowing for magnetic field alignment (a cylindrical bubble). However, a fully developed wedge, tilted toward the west and also field aligned, would be quite easy to penetrate on upleg and downleg. Since both of the Condor rockets penetrated such structures during both upleg and downleg, and because a nearly identical double penetration was observed during the PLUMEX I flight, the rocket data seem to support the wedge model.

We return now to the common cusplike feature associated with many of the JRO plumes. The straightforward explanation is that they correspond to wedges with strong scatter along the walls. The low backscatter levels in the cavity of these caps may be due to the low plasma density in this region, which has been drawn up from low altitudes, rather than a low turbulence level. (Radars respond to $\Delta n^2(\mathbf{k})$, not $[\Delta n(\mathbf{k})/n]^2$.) The uplift in such a cusp is far too rapid to be generated by a pure gravity wave induced electric field since such a field can be no greater than wB where w is the vertical neutral wind in the gravity wave and B the magnetic field. This has been pointed out previously [*Kelley et al.* 1981] and is discussed by *Argo and Kelley* [this issue]. The implication is that the generalized Rayleigh-Taylor process must be invoked to locally amplify the electric field associated with the seed structure. In reference to the previous discussion, the scale size for this amplification seems to be $\hat{k} \leq 1$, implying that velocity shear is an important factor.

4. SUMMARY OF THE CONDOR EQUATORIAL SPREAD F RESULTS

The key results are summarized in order of their presentation in the present series of papers beginning with the present paper.

Paper 1 (this paper). The combined rocket-radar data have been used to show that during rapid decreases of the scattering layer height over Jicamarca, the ionosphere is tilted such that the region to the west is lower than the adjacent region to the east. Such a configuration is shown to have a very high growth rate due to a wind-driven $\mathbf{E} \times \mathbf{B}$ instability ($\gamma \approx 3$ min^{-1}). These results verify previous conjectures concerning the tendency for multiple plumes to form in such a configuration. The case is further made that a characteristic separation distance exists between such plumes, which have a normalized $\hat{k} = k/2\pi L \approx 1$, where L is the zero-order vertical gradient scale length. This separation is consistent with a generalized Rayleigh-Taylor (or $\mathbf{E} \times \mathbf{B}$) instability which includes velocity shear. The magnitude of the required shear is larger than existing observations suggest, but higher localized shears may exist. The gentle undulations which have scales 5–6 times larger almost certainly must correspond to gravity wave induced effects. Further evidence that plumes are due to wedge-like features is also presented.

Paper 2 [LaBelle and Kelley, this issue]. Further evidence is presented to show that shallow spectral indices may at times characterize the spectral development in the intermediate-scale regime. In this context we define shallow to be a power law index of the form k^{-n} where n is less than 2. One reason that this result is important is that, to date, no computer simulation has yet yielded a spectral index shallower than k^{-2}. Until this experimental result is reproduced, one must question what aspect of the physics has been left out of the simulations. Several sources for the spectral form are investigated in paper 2. The nonlinear turbulence theory of *Sudan and Keskinen* [1984] predicts a $k^{-5/3}$ law which LaBelle and Kelley show quantitatively fits the data reasonably well, provided that a large anomalous diffusion coefficient is used (see also paper 3). The authors speculate that the turbulent cascade and $k^{-5/3}$ law applies when the exchange of energy between large and small eddies, which is measured by the nonlinear growth rate Γ, exceeds the energy input measured by the linear growth rate γ. The observed spectral forms even shallower than $k^{-5/3}$ are not explained by this argument. In addition to the comparison with nonlinear theory, LaBelle and Kelley point out two other processes which might elevate the relative power in the range near the 1-km scale and hence result in a shallower spectral slope at lower k. One such mechanism is an injection process due to wall turbulence driven by steep horizontal gradients. They show an example of wall turbulence which has a peak in $[\delta n(k)/n]^2$ near 1 km. The other process is similar but appeals to a lowering of the growth rate at k values above and below the 1-km scale by E region shorting of electric fields. Near 1 km the formation of images maintains the growth rate at a relatively high value.

Paper 3 [LaBelle et al., this issue]. The result based on PLUMEX data [*Kelley et al.*, 1982*a*; *Singh and Szuszczewicz*, 1984] that density fluctuation spectra display a very steep power law (k^{-5}) for wavelengths less than 100 m was verified in both Condor flights. The fact that the $E^2(k)$ spectrum measured simultaneously varies as k^{-3} was also verified and, taken together, strongly verifies the conjecture [*Kelley*, 1982] that drift waves, or at least some similar process involving finite $k_{\parallel}$, play an essential role in the evolution of equatorial spread F. Building upon this verification, LaBelle et al. show quantitatively that anomalous diffusion should occur because of the observed drift wave turbulence. The diffusion coefficient calculated fits the values needed to explain the balance of growth versus decay in the saturated turbulence spectra ob-

served in the Condor experiments. Typical values of the anomalous diffusion coefficient are in the range 200–500 m^2/s, which is 2 orders of magnitude higher than the collisional value. It is of interest to note that the same calculations applied to bottomside spread F and to low-altitude barium cloud power spectra reveal that the collisional diffusion coefficient is adequate to explain the results in such conditions. The implication is that an altitude (collision frequency?) threshold exists for onset of the anomalous diffusion effect. Curiously, the critical scale for onset of the steep spectral form becomes larger as the turbulence strength increases. This is opposite to what happens in neutral gas turbulence and may be related to the fact that the diffusion coefficient in a plasma process is k dependent.

Paper 4 [Basu et al., this issue]. Radar backscatter at 50 MHz, rocket, and VHF/GHz scintillation measurements of spread F irregularities at the magnetic equator in Peru were made during the Project Condor campaign in March 1983. It was found that the radar backscatter with extended plumes occurs, in association with the maximum values of 1.7-GHz scintillations. This established that the height-integrated electron density deviation of 200-m scale irregularities causing 1.7-GHz scintillations maximizes in extended 3-m plume structures. The magnitude of 1.7-GHz scintillations recorded at high elevation angles ($\sim 76°$) near the magnetic equator did not exceed a value of $S_4 = 0.2$ (4 dB) in contrast to the near-saturated 1.5-GHz scintillations routinely observed at Ascension Island near the crests of the equatorial anomaly of F_2 ionization. The observed scintillation magnitudes at 1.7 GHz have, however, been found to be compatible with the ambient F region and the irregularity parameters measured by the rockets. The spectral index n of scintillations was found to be shallow ($n \sim 3$) on March 1, 1983, when the F region was high, while the index was steep ($n \sim 5$) on March 14, 1983, when the F region was at a lower altitude. Curiously, the F region rocket measured nearly identical one-dimensional spectral indices of intermediate-scale irregularities on both evenings, which was compatible only with the shallower spectral index of the scintillations. The irregularity drift velocities measured by the spaced receiver scintillation measurements were in general agreement with the radar interferometer results except that the spaced-receiver drifts were 20% higher. The zonal drift was observed to be about 100 m/s when the F region was high and about 200 m/s when the F region was low. This result may be a consequence of the fact that the F region dynamo field at higher altitude above the magnetic equator becomes coupled with the off-equatorial locations through the earth's magnetic field and that the zonal neutral wind decreases with increasing latitude.

Paper 5 [Argo and Kelley, this issue]. As part of Project Condor a digital ionosonde was established at Huancayo, Peru. Five days of data were obtained, one simultaneous with Jicamarca VHF observations and a rocket flight. The direction-finding capability of the system coupled with the VHF data has given clearer insight into operation of the ionosonde system and its equatorial spread F in general. A modified phenomenology is developed which uses the radar's ability to do echo location. The onset of irregularities is seen to occur in the east and to move westward, while inside this large-scale structure the plasma is found to drift eastward. A very curious difference has been identified between spread F observations with the HF radar and with the VHF radar at Jicamarca. At VHF, spread F onset often occurs when the ionosphere is rising, whereas in all five examples presented here, the digital ionosonde detected onset when the apparent ionosphere motion was downward. The effect could be instrumental but may be related to the considerable orographic differences in the two sites. Isolated scattering patches are observed and tentatively identified as detached or "fossil" plumes. Additional evidence is presented that acoustic gravity waves play an important role in equatorial spread F.

Paper 6 [Meriwether et al., this issue]. Nighttime measurements of equatorial thermospheric wind dynamics at Arequipa, Peru, were made with an automated field-widened Fabry-Perot interferometer between April 1983 and August 1983. Data have been reduced for 62 nights. Significant seasonal variations in both zonal and meridional components of the thermospheric neutral wind vector were observed near the equinox. Between 2000 and 2300 LT the zonal wind component is eastward with an amplitude between 100 and 150 m/s that gradually ebbs to zero by dawn. The meridional component is generally small throughout the night. In the winter months (May–August) and at the winter solstice the zonal wind persists eastward throughout the night with speeds between 50 and 150 m/s. The meridional component is directed poleward (southward) toward the winter hemisphere with a speed of 50–75 m/s that decays to zero by midnight. Comparison with the predictions of the National Center for Atmospheric Research thermospheric general circulation model (TGCM) for equinoctial and solstice conditions shows good agreement. We conclude that the observed seasonal changes are caused by the changing nature of the solar forcing functions. The Arequipa results indicate that the day-to-day variability in the winter thermospheric winds is less than that found for the summer equatorial observations obtained at Kwajalein.

Acknowledgments. The experiments described here were all part of the Condor campaign, a joint undertaking by the National Aeronautics and Space Administration, the National Science Foundation, and their counterparts in Peru, the Comission Nacional de Investigacion y Desarrollo Aerospacial and the Instituto Geofisico del Peru. In addition, significant contributions to the effort were made by the Los Alamos National Laboratory, the Air Force Geophysics Laboratory, and the CNRS of France.

The Editor thanks R. T. Tsunoda and another referee for their assistance in evaluating this paper.

REFERENCES

Aarons, J., J. P. Mullen, H. E. Whitney, and E. M. E. MacKenzie, The dynamics of equatorial irregularity patch formation, motion, and decay, *J. Geophys. Res., 85*, 139, 1980.

Argo, P. E., and M. C. Kelley, Digital ionosonde observations during equatorial spread F, *J. Geophys. Res.*, this issue.

Baker, K. D., E. F. Pound, and J. C. Ulwick, Digital plasma frequency probe for fine scale ionospheric measurements, in *Small Rocket Instrumentation Techniques*, edited by K. Maeda, p. 49, North Holland, Amsterdam, 1969.

Baker, K. D., J. LaBelle, R. F. Pfaff, L. C. Howlett, N. B. Rao, J. C. Ulwick, and M. C. Kelley, Absolute electron density measurements in the equatorial ionosphere, *J. Atmos. Terr. Phys., 47*, 781, 1985.

Balsley, B. B., G. Haerendel, and R. A. Greenwald, Equatorial spread F: Recent observations and a new interpretation, *J. Geophys. Res., 77*, 5625, 1972.

Basu, S., and H. E. Whitney, The temporal structure of intensity scintillations over the magnetic equator, *Radio Sci., 18*, 263, 1983.

Basu, S., Su. Basu, J. Aarons, J. P. McClure, and M. D. Cousins, On the coexistence of kilometer and meter scale irregularities in the nighttime equatorial F region, *J. Geophys. Res., 83*, 4219, 1978.

Basu, S., Su. Basu, J. LaBelle, E. Kudeki, B. G. Fejer, M. C. Kelley, H. E. Whitney, and A. Bushby, Gigahertz scintillations and spaced

receiver drift measurements during Project Condor equatorial F region rocket campaign in Peru, *J. Geophys. Res.*, this issue.

Basu, Su., and S. Basu, Equatorial scintillations: Progress since ISEA-6, *J. Atmos. Terr. Phys.*, *47*, 753, 1985.

Basu, Su., S. Basu, J. P. McClure, W. B. Hanson, and H. E. Whitney, High-resolution topside in situ data of electron densities and VHF/GHz scintillation in the equatorial region, *J. Geophys. Res.*, *88*, 403, 1983.

Bhavsar, P. D., K. Ramanvjaro, and K. G. Verenekar, Study of the neutral upper atmosphere winds near the equator, *Space Res., V*, 986, 1965.

Costa, E., and M. C. Kelley, On the role of steepened structures and drift waves in equatorial spread *F*, *J. Geophys. Res.*, *83*, 4359, 1978.

Farley, D. T., B. B. Balsley, R. F. Woodman, and J. P. McClure, Equatorial spread *F*: Implications of VHF radar observations, *J. Geophys. Res.*, *75*, 7199, 1970.

Fejer, B. G., and M. C. Kelley, Ionospheric irregularities, *Rev. Geophys.*, *18*, 401, 1980.

Fejer, B. G., D. T. Farley, B. B. Balsley, and R. F. Woodman, Vertical structure of the VHF backscattering region in the equatorial electrojet and the gradient drift instability, *J. Geophys. Res.*, *80*, 1313, 1975.

Fejer, B. G., D. T. Farley, R. F. Woodman, and C. Calderon, Dependence of equatorial *F* region vertical drifts on season and solar cycle, *J. Geophys. Res.*, *84*, 5792, 1979.

Fejer, B. G., E. Kudeki, and D. T. Farley, Equatorial *F* region zonal plasma drifts, *J. Geophys. Res.*, *90*, 12,249, 1985.

Guzdar, P. N., P. Satyanarayana, J. D. Huba, and S. L. Ossakow, Influence of velocity shear on the Rayleigh-Taylor instability, *Geophys. Res. Lett.*, *9*, 547, 1982.

Hanson, W. B., and D. K. Bamgboye, The measured motions inside equatorial plasma bubbles, *J. Geophys. Res.*, *89*, 8997, 1984.

Kelley, M. C., Nonlinear saturation spectra of electric fields and density fluctuations in drift wave turbulence, *Phys. Fluids*, *25*, 1002, 1982.

Kelley, M. C., Equatorial spread *F*: Recent results and outstanding problems, *J. Atmos. Terr. Phys.*, *47*, 745, 1985.

Kelley, M. C., and J. P. McClure, Equatorial spread-*F*: A review of recent experimental results, *J. Atmos. Terr. Phys.*, *43*, 427, 1981.

Kelley, M. C., and E. Ott, Two-dimensional turbulence in equatorial spread *F*, *J. Geophys. Res.*, *83*, 4369, 1978.

Kelley, M. C., G. Haerendel, H. Kappler, A. Valenzuela, B. B. Balsley, D. A. Carter, W. L. Ecklund, C. W. Carlson, B. Hausler, and R. Torbert, Evidence for a Rayleigh-Taylor type instability and upwelling of depleted density regions during equatorial spread *F*, *Geophys. Res. Lett.*, *3*, 448, 1976.

Kelley, M. C., M. F. Larsen, C. LaHoz, and J. P. McClure, Gravity wave initiation of equatorial spread *F*: A case study, *J. Geophys. Res.*, *86*, 9087, 1981.

Kelley, M. C., R. Pfaff, K. D. Baker, J. C. Ulwick, R. C. Livingston, C. L. Rino, and R. T. Tsunoda, Simultaneous rocket probe and radar measurements of equatorial spread *F*: Transitional and short-wavelength results, *J. Geophys. Res.*, *87*(A3), 1575, 1982*a*.

Kelley, M. C., R. C. Livingston, C. L. Rino, and R. T. Tsunoda, The vertical wave number spectrum of topside equatorial spread *F*: Estimates of backscatter levels and implications for a unified theory, *J. Geophys. Res.*, *87*, 5217, 1982*b*.

Klostermeyer, J., Nonlinear investigation of the spatial resonance effect in the nighttime equatorial *F* region, *J. Geophys. Res.*, *83*, 3753, 1978.

Kudeki, E., B. G. Fejer, D. T. Farley, and H. M. Ierkic, Interferometer studies of equatorial *F* region irregularities and drifts, *Geophys. Res. Lett.*, *8*, 377, 1981.

LaBelle, J., and M. C. Kelley, The generation of kilometer scale irregularities in equatorial spread *F*, *J. Geophys. Res.*, this issue.

LaBelle, J., M. C. Kelley, and C. E. Seyler, An analysis of the role of drift waves in equatorial spread *F*, *J. Geophys. Res.*, this issue.

Livingston, R. C., C. L. Rino, J. P. McClure, and W. B. Hanson, Spectral characteristics of medium-scale equatorial *F* region irregularities, *J. Geophys. Res.*, *86*, 2421, 1981.

Mendillo, M., and A. Tyler, Geometry of depleted plasma regions in the equatorial ionosphere, *J. Geophys. Res.*, *88*, 5778, 1983.

Meriwether, J. W., Jr., J. W. Moody, M. A. Biondi, and R. G. Roble, Optical interferometric measurements of nighttime equatorial thermospheric winds at Arequipa, Peru, *J. Geophys. Res.*, this issue.

Morse, F. A., B. C. Edgar, H. C. Koons, C. J. Rice, W. J. Heikkila, J. H. Hoffman, B. A. Tinsley, J. D. Winningham, A. B. Christensen, R. F. Woodman, J. Pomalaza, and R. N. Teixeira, Equion, an equatorial ionospheric irregularity experiment, *J. Geophys. Res.*, *82*, 578, 1977.

Ossakow, S. L., Spread *F* theories—A review, *J. Atmos. Terr. Phys.*, *43*, 437, 1981.

Rino, C. L., R. T. Tsunoda, J. Petriceks, R. C. Livingston, M. C. Kelley, and K. D. Baker, Simultaneous rocket-borne beacon and in situ measurements of equatorial spread *F*: Intermediate wavelength results, *J. Geophys. Res.*, *86*, 2411, 1981.

Röttger, J., Wave like structures of large scale equatorial spread *F* irregularities, *J. Atmos. Terr. Phys.*, *35*, 1195, 1973.

Satyanarayana, P., P. N. Guzdar, J. D. Huba, and S. L. Ossakow, Rayleigh-Taylor instability in the presence of a stratified shear layer, *J. Geophys. Res.*, *89*, 2945, 1984.

Singh, M., and E. P. Szuszczewicz, Composite equatorial spread *F* wave number spectra from medium to short wavelengths, *J. Geophys. Res.*, *89*, 2313, 1984.

Sipler, D. P., and M. A. Biondi, Equatorial *F* region netural winds from nightglow OI 630.0 nm Doppler shifts, *Geophys. Res. Lett.*, *5*, 373, 1978.

Sudan, R. N., and M. J. Keskinen, Unified theory of the power spectrum of intermediate wavelength ionospheric electron density fluctuations, *J. Geophys. Res.*, *89*, 9840, 1984.

Szuszczewicz, E. P., R. T. Tsunoda, R. Narcisi, and J. C. Holmes, Coincident radar and rocket observations of equatorial spread-*F*, *Geophys. Res. Lett.*, *7*, 537, 1980.

Tsunoda, R. T., Time evolution and dynamics of equatorial backscatter plumes, 1, Growth phase, *J. Geophys. Res.*, *86*, 139, 1981.

Tsunoda, R. T., On the generation and growth of equatorial backscatter plumes, 2, Structuring of the west walls of upwellings, *J. Geophys. Res.*, *88*, 4869, 1983.

Tsunoda, R. T., R. C. Livingston, and C. L. Rino, Evidence of a velocity shear in bulk plasma motion associated with the post-sunset rise of the equatorial *F*-layer, *Geophys. Res. Lett.*, *8*, 807, 1981.

Tsunoda, R. T., R. C. Livingston, J. P. McClure, and W. B. Hanson, Equatorial plasma bubbles: Vertically elongated wedges from the bottomside *F* layer, *J. Geophys. Res.*, *87*, 9171, 1982.

Whitney, H. E., Notes on the relationship of scintillation index to probability distributions and then uses for system design, *Rep. AFCRL-TR-74-0004*, Air Force Cambridge Res. Lab., Bedford, Mass., 1974.

Whitney, H. E., J. Aarons, and C. Malik, A proposed index for measuring ionospheric scintillations, *Planet. Space Sci.*, *17*, 1069, 1969.

Woodman, R. F., Vertical drift velocities and east-west electric fields at the magnetic equator, *J. Geophys. Res.*, *75*, 6249, 1970.

Woodman, R. F., and C. LaHoz, Radar observations of *F* region equatorial irregularities, *J. Geophys. Res.*, *81*, 5447, 1976.

Zalesak, S. T., S. L. Ossakow, and P. K. Chaturvedi, Nonlinear equatorial spread *F*: The effect of neutral winds and background Pedersen conductivity, *J. Geophys. Res.*, *87*, 151, 1982.

P. Argo, Atmospheric Sciences Group, Earth and Space Sciences Division, Los Alamos National Laboratory, Los Alamos, NM 87545.

K. D. Baker, CASS, Utah State University, Logan, UT 84332.

Santimay Basu, Air Force Geophysics Laboratory, Hanscom Air Force Base, MA 01731.

Sunanda Basu, Emmanuel College, Boston, MA 02115.

D. T. Farley, B. G. Fejer, M. C. Kelley, J. LaBelle, and W. E. Swartz, School of Electrical Engineering, Cornell University, Ithaca, NY 14853.

C. Hanuise, LSEET/CNRS, University of Toulon, 639 Boulevard des Armaris, 83100 Toulon, France.

E. Kudeki, Department of Electrical Engineering, University of Illinois, Urbana, IL 61801.

J. W. Meriwether, Jr., Space Physics Research Laboratory, University of Michigan, Ann Arbor, MI 48109.

R. F. Woodman, Institute Geofisico del Peru, Apartado 3747, Lima 100, Peru.

(Received June 17, 1985;
revised October 4, 1985;
accepted November 21, 1985.)